Wave-front dislocations in the soundfield of a pulsed circular piston radiator

Francis J. Wright[a] and Michael V. Berry
H. H. Wills Physics Laboratory, University of Bristol, Tyndall Avenue, Bristol, BS8 1TL, United Kingdom

(Received 1 May 1983; accepted for publication 2 October 1983)

Wave-front dislocations are lines in space along which wave fronts end, named by analogy with dislocations in imperfect crystals. Continuous waves and quasimonochromatic pulses (of continuous waves with slowly varying envelopes) are conveniently represented by complex-valued wavefunctions, the zeros of which correspond to wave-front dislocations. Pulse dislocations move through the wavefield, and may interact, as the pulse propagates. As examples of realistic model wavefields, the soundfields of a rigid circular piston radiator vibrating in a fixed rigid baffle plane, driven both by a sinusoidal source producing continuous waves and by this source modulated by a Gaussian envelope, are computed exactly and displayed. The birth of dislocations in the nearfield and their propagation with the pulse into the farfield are observed and discussed, and birth and death events in the nearfield are displayed in detail. The behavior of quasimonochromatic pulses and their dislocations may be understood in terms of the carrier wavefield, both qualitatively and, via a perturbation theory, quantitatively.

PACS numbers: 43.20.Rz, 43.20.Bi

INTRODUCTION

Some of the finest detail of a wavefield is embodied in its wave-front dislocations. These are lines in space on which wave fronts end, named by analogy with crystal dislocations along which atomic planes end. In a continuous wavefield the dislocation lines are fixed, but in a wavefield with nontrivial time variation the dislocation lines generally move, and may interact, as do crystal dislocations.

Wave-front dislocations were discovered by Nye and Berry[1] in ultrasound reflected from a rough surface. The incident wave was a pulse of sinusoidal waves with a slowly varying envelope, and the reflected wave, received at a point and displayed on an oscilloscope as sound pressure against time, was an extended train of disorderly oscillations. On moving the receiver to explore the wave at different places, it was quite common to observe two wavecrests move apart and an extra crest appear between them, or the time-reversed sequence of events. The meaning of such a birth or death of a wavecrest is that a dislocation line has intersected the track of the receiver. These phenomena are discussed in more detail, illustrated, and the basic theory developed, by Nye and Berry[1]; wave-front dislocations are set in a more general context by Berry.[2]

The ultrasonic experiments were devised as laboratory analogs for radio echo sounding of polar ice sheets. The echo, and especially its skeleton of dislocation lines, provides a three-dimensional reference frame, fixed relative to the bedrock, with respect to which displacements can be measured. Radio echo-sounding experiments[3] in Antarctica suggest that displacements as small as a hundredth of a wavelength can be measured in this way. In their own right, ultrasonic pulses are used extensively in medicine, NDT, etc. From a theoretical point of view these applications are quite crude; usually, only the times of emission and reception of the pulse as a whole are recorded, and interference effects arising from the presence of several waves within the pulse envelope are ignored. In any precise quantitative interpretation of an echo, however, a precondition would be a complete understanding of the wavefield in the emitted pulse, dislocations and all—hence the study reported here.

Wave fronts are geometrical abstractions of a wavefield and their precise definition can be made in several ways. Following Nye and Berry, our choice is to work with a complex-scalar-valued wavefunction $\psi(\mathbf{r},t)$. This can be written in amplitude-phase form as

$$\psi(\mathbf{r},t)=\rho(\mathbf{r},t)e^{i\chi(\mathbf{r},t)}, \tag{1}$$

where ρ and χ are real-scalar-valued functions, which are *uniquely* determined (mod 2π for χ) unless $\psi=0$, in which case χ is indeterminate. In this representation we *define* the family of wave fronts to be the surfaces in space satisfying

$$\chi(\mathbf{r},t)=c \quad \text{modulo } 2\pi,$$

for some constant c, usually taken as zero. The wave fronts are undefined when χ is indeterminate, i.e., when $\psi=0$, and wave fronts end along lines on which ψ has a simple zero; this defines the wave-front dislocation lines. (Higher order zeros correspond to dislocation interactions.) In a transverse section through a dislocation the equiphase lines ($\chi=$ const) have a characteristic radial pattern, and the ending wave front corresponds to *one* of the radial spokes [see Figs. 4(b) and 6 later, and also Ref. 1].

For the analogy with crystal dislocations to be useful there should be a number of wave fronts in the neighborhood of the dislocation which are not too contorted. In particular, the envelope function should be nonzero over at least several periods of the carrier. We expect the dislocation structure of

[a] Present address: Department of Applied Mathematics, Queen Mary College, University of London, Mile End Road, London E1 4NS, UK. For year 1983–1984 on Sabbatical at Institut für Informationsverarbeitung, Köstlinstr. 6, D-7400 Tübingen, West Germany.

 0001-4966/84/030733-16$00.80

a wavefield to be simplest when the modulation is slowly varying in comparison with the carrier, which we will call the *quasimonochromatic* (qm) case. Many real remote sensing systems generate qm wavefields (which are often analyzed as though they were monochromatic!). Discussion of dislocations to date has concentrated on quasimonochromaticity, and we shall do so here, although we anticipate that wave-front dislocations would be a useful concept in any wave system where wave fronts could be sensibly defined.

Only *real* wavefunctions are usually observed, but Nye[4] has shown that in the quasimonochromatic limit it is possible to reconstruct the complex wavefunction from its real part alone. This ability has been realized experimentally in a "complex-plane wavefunction display" by Walford *et al.*[5] It is also possible to define wave fronts and wave-front dislocations using only a real wavefunction[6] by analogy with the way wavefunctions would typically be observed on an oscilloscope, but observationally we would not expect this definition to give results significantly different from those based on a complex wavefunction.

Nye and Berry[1] set up *local* models of dislocated wavefields in order to prove that they could exist and to demonstrate their basic properties, and the local properties of wave-front dislocations have recently been defined more rigorously by Nye.[4] The effect of pulse shape on the motion of dislocations has been discussed by Wright and Nye[7] for three simple symmetrical examples—Gaussian, Lorentzian, and hyperbolic secant—and also for a "smooth-step" envelope. This was primarily in the context of a simple two-beam model wavefield involving linear spatial modulation, which again is physically realizable only locally. These authors also introduced a bandwidth-perturbation theory for predicting the behavior of dislocations in quasimonochromatic wavefields from continuous wave (cw) data alone.

The purpose of the present paper is to study the wave-front dislocations in a *realistic global* model of a simple physical wave system. We chose to investigate numerically the soundfield of a rigid plane circular piston set in a rigid infinite plane baffle. The rotation symmetry of this system makes it essentially two-dimensional, so that the wavefield is easy to display. It also means that the dislocation lines must be circular loops centered on, and perpendicular to, the axis and must lie in the wave-front surfaces so that only dislocations of "pure-edge" type[1,2,4] can occur. This model radiator has been studied by other authors. However, they have either computed only cw fields (e.g., Refs. 8–11) or they have not presented their data so as to show the wave-front dislocations in studies of pulsed fields (e.g., Ref. 12).

The details of our model and the resulting diffraction integral are discussed in Sec. I and Appendices A and B. The parameters were chosen mainly to match experimental observations of dislocations by Nye, Walford (unpublished), and Humphrey.[13] In Sec. II, we analyze the continuous wavefield for one particular frequency in order to set the scene for Sec. III, in which we modulate the amplitude of this cw source to give a single pulse with a Gaussian envelope and observe the dislocation structure as the pulse propagates through the soundfield. We look more closely in Sec. IV at the dislocation interactions which have occurred. In Sec. V we summarize these observations in terms of the trajectory surface traced out by the moving dislocation lines and relate these to the results of the perturbation theory of Wright and Nye.[7] Section VI draws together our conclusions.

Our discussion is relevant to fields other than acoustics. For example, in communications engineering considerable interest exists in the "synthesis of antenna patterns with prescribed nulls,"[14] which we can paraphrase as "designing wavefields with specified wave-front dislocation trajectories." This problem is normally analyzed in terms of farfield cw nulls only.

I. THE CIRCULAR PISTON RADIATOR MODEL

The soundfield we consider is generated by a rigid plane circular piston of radius a vibrating in an infinite rigid plane baffle, such that its displacement from the baffle plane at time t is $F(t)$. We use a cylindrical polar coordinate system such that the baffle plane is given by $z = 0$, and we consider the soundfield in the half-space $z > 0$. We denote by ρ the perpendicular distance of the field point from the z axis, as in Fig. 1.

We assume that the soundfield may be represented by a velocity potential ψ, which we shall take as our scalar wavefunction, such that the irrotational fluid velocity is given by $\mathbf{u} = -\nabla\psi$ and ψ satisfies the nondispersive scalar wave equation

$$c^2\nabla^2\psi = \frac{\partial^2\psi}{\partial t^2},$$

where c is the constant sound velocity. Then from standard hydrodynamics[15] the acoustic pressure and density fluctuations are, respectively,

$$\delta p = d\frac{\partial\psi}{\partial t} \quad \text{and} \quad \delta d = \frac{\delta p}{c^2},$$

where d is the mean fluid density, so that ψ completely determines the soundfield.

The boundary condition on the fluid is that its normal velocity equals that of the boundary. Assuming $F(t)$ to be sufficiently small to justify applying this boundary condition at $z = 0$, the boundary condition becomes

$$u_z(\rho, 0) \equiv -\frac{\partial\psi}{\partial z}(\rho, 0) = \begin{cases} F'(t) & \rho < a \\ 0 & \rho > a \end{cases},$$

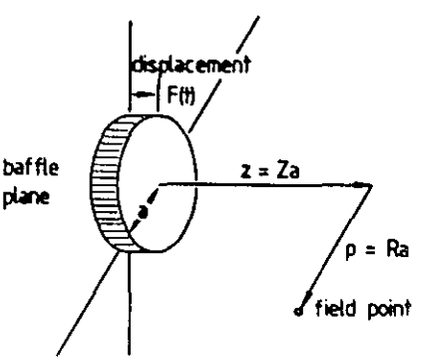

FIG. 1 Coordinates for the wavefield

where $F'(t) \equiv dF/dt$. This completely specifies the wavefunction, for which a convenient representation is

$$\psi(\rho, z, t) = \Theta(a-\rho)cF(t-z/c) + \frac{ac}{\pi}\int_0^{\pi} d\varphi \left(\frac{\rho\cos\varphi - a}{a^2+\rho^2-2a\rho\cos\varphi}\right) \times F[t-(z^2+a^2+\rho^2-2a\rho\cos\varphi)^{1/2}/c], \quad (2)$$

where

$$\Theta(x) = \begin{cases} 0 & \text{if } x<0 \\ \frac{1}{2} & \text{if } x=0 \\ 1 & \text{if } x>0 \end{cases}$$

The derivation of this integral is sketched and discussed briefly in Appendix A. It is *exact* for *any* field point position (ρ, z) and for an arbitrary piston displacement function $F(t)$. At first sight one might suspect it to predict that ψ is discontinuous at $\rho = a$; however, closer examination shows that this is not the case. The integrand is regular (assuming F to be regular), and is easily evaluated numerically using conventional routines.[16] Note that since the acoustic pressure is $\delta p = d\partial\psi/\partial t$, the above formula gives essentially δp if we regard $F(t)$ as piston velocity rather than displacement. This observation facilitates comparison of our results with those of other authors.

On the axis (2) reduces trivially to

$$\psi(0, z, t) = c\{F(t-z/c) - F[t-(z^2+a^2)^{1/2}/c]\}, \quad (3)$$

which is well known.[17–19] On the cylinder generated by the edge of the piston, (2) also simplifies somewhat to

$$\psi(a, z, t) = \frac{c}{2}\left(F(t-z/c) - \frac{1}{\pi}\int_0^{\pi} d\varphi \times F\{t-[z^2+2a^2(1-\cos\varphi)]^{1/2}/c\}\right). \quad (4)$$

This form is convenient numerically to avoid the indeterminacy of the integrand of (2) at $\varphi = 0$ when $\rho = a$.

Converting to spherical polar coordinates r and θ such that $\rho = r\sin\theta$ and $z = r\cos\theta$ we find the farfield limit, i.e., the limiting form as $r \to \infty$, to be

$$\psi_F(r, \theta, t) = \frac{ac}{\pi r\sin\theta}\int_0^{\pi} d\varphi\cos\varphi \times F\left(t - \frac{r}{c} + \frac{a}{c}\sin\theta\cos\varphi\right) + O\left(\frac{1}{r^2}\right) \quad (5)$$

in agreement with elementary Fraunhofer diffraction theory. On the axis $\theta = \rho = 0$ and (5) is indeterminate, but its limiting form as $\theta \to 0$ gives

$$\psi_F(r, 0, t) = (a^2/2r)F'(t-r/c) \quad (6)$$

assuming F to be at least once differentiable. This agrees with the limiting form of (3) as $z \to \infty$. Comparing (3) and (6) suggests that in the *nearfield* the velocity potential is related to the piston *displacement*, whereas in the *fairfield* it is related to the piston *velocity*.

II. THE CONTINUOUS WAVEFIELD AND ITS NULLS

Not surprisingly, a quasimonochromatic wavefield is best understood by relating it to the continuous wavefield at its carrier frequency. Therefore, in this section we examine the particular continuous wavefield which we intend to modulate in the next section, paying particular attention to its (fixed) wave-front dislocations or nulls. The linearity of the theory allows us to use complex wavefunctions and piston displacements, as discussed in the Introduction. Therefore we drive the piston with the monochromatic signal

$$F(t) = e^{i\omega t}$$

of angular frequency ω, and for convenience define the dimensionless variables

$$R = \rho/a, \quad Z = z/a, \quad T = \omega t, \quad K = ka = \omega a/c,$$

and

$$\Psi(R, Z, T) = (1/c)\psi(\rho, z, t).$$

The monochromatic wavefunction becomes, from (2),

$$\Psi_m(R, Z, T) = \Theta(1-R)e^{i(T-KZ)} + \frac{1}{\pi}\int_0^{\pi} d\varphi\left(\frac{R\cos\varphi - 1}{1+R^2-2R\cos\varphi}\right) \times \exp\{i[T-K(Z^2+1+R^2 - 2R\cos\varphi)^{1/2}]\}. \quad (7)$$

On the axis this reduces to

$$\Psi_m(0, Z, T) = e^{iT}(e^{-iKZ} - e^{-iKZ_1}) = 2ie^{i(T-KZ')}\sin[K(Z_1-Z)/2],$$

where $Z_1 = (Z^2+1)^{1/2}$ and $Z' = [Z+(Z^2+1)^{1/2}]/2$ is the mean distance of the field point from the center and edge of the piston. Axial nulls occur at finite Z when

$$K(Z_1 - Z)/2 = n\pi \quad \text{for some integer } n>0,$$
$$\text{i.e., at } Z = [K^2 - (2n\pi)^2]/4n\pi K.$$

Since this must be >0 there are exactly $\text{int}(K/2\pi)$ axial nulls, where $\text{int}(x) \equiv \max\{0, \text{integer} < x\}$. In fact, this is the number of whole wavelengths λ which fit into the piston radius a, because $K/2\pi = a/\lambda$.

The farfield limit simplifies to

$$\psi_{Fm}(r, \theta, t) = ie^{i(\omega t - kr)}(ac/r\sin\theta)J_1(ka\sin\theta)$$

on recognizing the integral representation of the Bessel function J_1 (Abramowitz and Stegun,[20] formula 9.1.21). This is a standard result[21] [usually calculated for $F'(t) = e^{i\omega t}$], showing that the maximum farfield amplitude occurs on the axis, where

$$\psi_{Fm}(r, 0, t) = i\omega e^{i(\omega t - kz)}(a^2/2r).$$

Therefore, we define the normalized farfield wavefunction

$$\Psi_{Fm}(\theta, \tau) = \frac{2r}{\omega a^2}\psi_{Fm}(r, \theta, t) = ie^{i\tau}\frac{2J_1(K\sin\theta)}{K\sin\theta}, \quad (8)$$

where $K = ka$ as above and we have introduced the dimensionless retarded time $\tau = \omega t - kr$.

Farfield (angular) nulls occur at $K\sin\theta = j_{1,n}$, where $j_{1,n}$ is the nth zero of J_1 and has the value $(n+\frac{1}{4})\pi$ asymptotically as $n \to \infty$. The first few values are shown in Table I, using information from Abramowitz and Stegun.[20] If $j_{1,n} < K < j_{1,n+1}$ there are n farfield nulls, i.e., approximately

TABLE I. Exact and approximate zeros of the Bessel function J_1

n	$j_{1,n}$	$(n+\frac{1}{4})\pi$
1	3.832	3.927
2	7.016	7.069
3	10.173	10.210
4	13.324	13.352
5	16.471	16.493

int$(K/\pi - \frac{1}{4})$, which may underestimate the true number by at most 1.

We conjecture that cw nulls are unlikely other than on the axis or at infinity; there are no others for the value of K that we have used. It would be interesting to plot the trajectories of the cw nulls in this model as K varies, but we have not done so here and are not aware that anyone else has. We shall see later that the relation between axial and farfield cw nulls is important in understanding the pulse dislocations. Because

$$\text{int}(K/\pi - \tfrac{1}{4}) = 2\,\text{int}(K/2\pi) \pm 1 \quad \text{for } K \geq 0,$$

the number of farfield nulls is approximately twice the number of axial nulls, with an error of at most $+1$ to -2.

For our numerical study we took $K = 10.0$ (i.e., $\lambda/a = 0.63$), mainly to model the observations mentioned in the Introduction, which used pulses of ultrasound in air ($c = 331.5\ \text{ms}^{-1}$) with a carrier frequency of about 100 kHz ($\lambda \simeq 0.33$ cm) and a piston radius a of about 0.5 cm. This value of K gives only *one axial null* at $Z = 0.4816$ and *two farfield nulls* at $\theta = 22.53°$ and 44.55°. This cw field has sufficient structure to give interesting dislocations in the pulse case while remaining sufficiently simple to understand. An important observation is that for a slightly larger value of K a new farfield null would appear at $\theta = 90°$ (without immediately introducing a new axial null, thereby exploiting the error limit that the number of farfield nulls may be twice the number of axial nulls $+1$). As expected, there are vestiges of this incipient null in the diffraction pattern.

Results are displayed first for the farfield, which is simpler than the nearfield. Figure 2(a) shows the reduced farfield amplitude $|\Psi_{Fm}|$ as a function of θ, and Fig. 2(b) shows a set of equiphase lines in (θ, τ) space, both calculated from (8). The incipient null is evident from the very low amplitude at $\theta = 90°$. Because of the factor i in (8) it is convenient to use "phase $= \pi/2$ mod 2π" to represent wave fronts, as in Fig. 2(b). This figure is trivial, but is useful for comparison with the pulse case later. The wave fronts are straight lines broken up into an "interlocking comb" pattern, caused by the phase jumps of π when J_1 changes sign through the nulls. This pattern is typical of a null *surface* (degenerate dislocation), which occurs in the farfield because r plays only a trivial role.

The nearfield wavefunction computed from (7) is shown in Fig. 3. Figure 3(a) shows the amplitude as a surface in three dimensions, and Fig. 3(b) shows it as a contour plot. Note that $|\Psi_m|$ has a maximum value of 2. Figure 3(c) shows the equiphase lines in steps of $\pi/4$ from 0, so that every eighth may be taken to represent a wave front. In all our

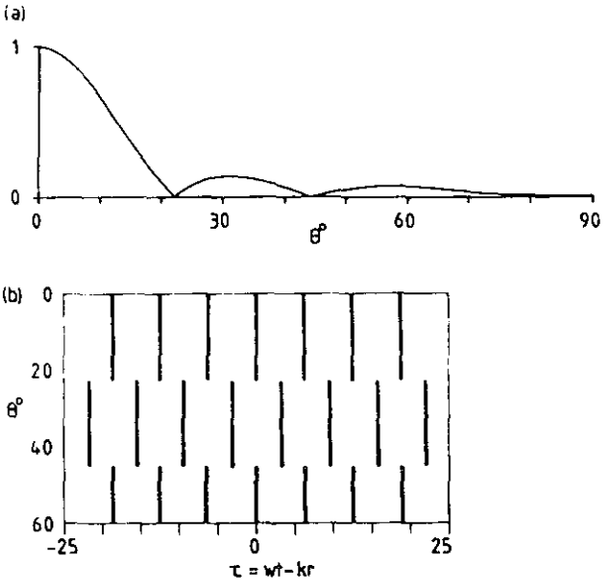

FIG. 2. Reduced farfield continuous wavefunction: (a) amplitude; (b) equiphase lines at $\pi/2$ mod 2π, for comparison with the pulse case shown in Fig. 4(b).

nearfield plots the complete wavefield is generated by rotating the section plotted through 360° about the axis of the system, which is the *top line* bounding the plots. The radius of the piston is indicated by the double line at the top left of the plots running along $Z = 0$ from $R = 0$ to $R = 1$; R increases downwards.

The phase singularity at a dislocation, discussed in the Introduction, shows up clearly at the axial null in Fig. 3(c), but note that this is a degenerate null because of the axial symmetry. The amplitude "landscape" shows valleys, whose bottoms are generally not at zero height, two of which run off into the farfield. One valley begins at the axial null, runs up to a saddle point at about $Z = 0.9$, $R = 0.3$, and then runs down into the farfield with monotonically decreasing height, which becomes zero at infinity. The other main valley begins at a minimum just in front of the piston, near $Z = 0.1$, $R = 0.4$, runs up to a saddle point near $Z = 0.25$, $R = 0.6$, and then down into the farfield. The two minima are linked by a short valley passing over the saddle near $Z = 0.25$, $R = 0.25$. The curvature of the contours close to the piston near $R = 1$ in Fig. 3(b) suggests another slight valley, and Fig. 3(a) clearly shows a slight dip here: this is the vestige of the next farfield null (and associated valley) which would appear if K were increased. Figure 3(b) and (c) shows the farfield null angles as chain lines. Note that Fig. 3(c) shows the equiphase lines bunching together in the minima near the piston, tending towards the coalescence which occurs at an actual null.

Figure 3(d) and (e) shows the actual wavefunctions, one with a phase shift of $\pi/2$ relative to the other. The solidi on all three-dimensional plots mark the zero crossings. Figure 3(e) shows particularly clearly the effect of the axial null, where a wavecrest comes to an abrupt end. Bearing in mind that the graphs should be rotated about the axis to generate the full wavefield, the effect is that the wave fronts develop a

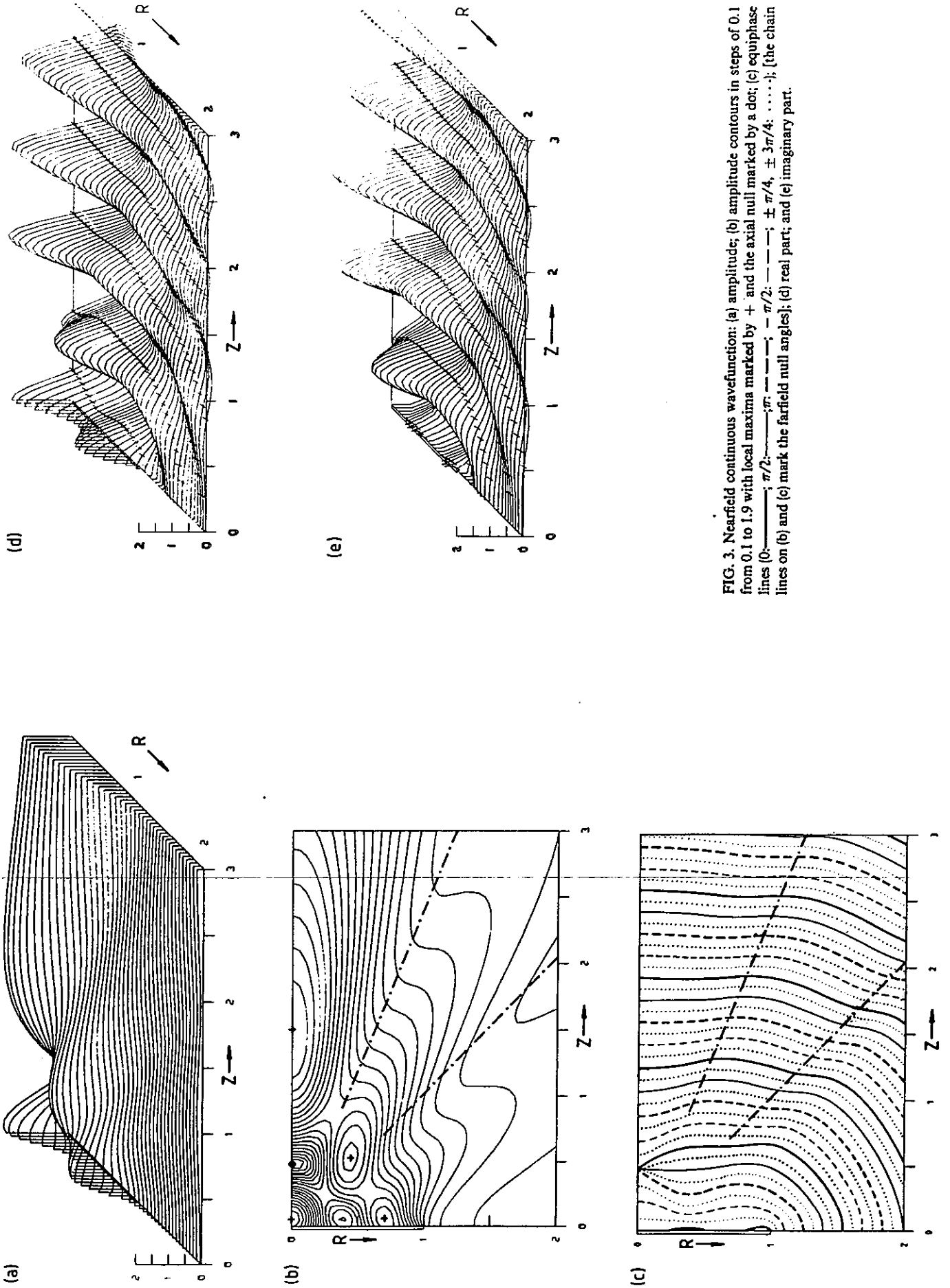

FIG. 3. Nearfield continuous wavefunction: (a) amplitude; (b) amplitude contours in steps of 0.1 from 0.1 to 1.9 with local maxima marked by + and the axial null marked by a dot; (c) equiphase lines (0: ——; $\pi/2$: — — —; π: — — —; $-\pi/2$: — — —; $\pm\pi/4$, $\pm 3\pi/4$: · · · · ·); [the chain lines on (b) and (c) mark the farfield null angles]; (d) real part; and (e) imaginary part.

puncture as they pass through the null, which immediately closes again on the other side. The point puncture is fixed in space and the wave fronts sweep through it.

Figure 3 shows what look like approximately standing waves across the piston face, with every point over the piston face nearly in phase at any fixed time [see Fig. 3(c)], but the wavelength seems to be somewhat longer than the real wavelength. The complicated diffraction effects seem to be contained within a sphere of radius about $1.5a$ around the center of the piston. Outside this radius the amplitude is decreasing monotonically, and the wave fronts (or equiphase lines) look like distorted spherical waves. This distortion takes the form of kinks near the farfield null angles, which are tending towards the farfield discontinuities shown in Fig. 2(b).

It is reasonable in practice to regard the farfield as where the cw amplitude decreases monotonically with distance from the piston center. Then along the axis the nearfield/farfield "boundary" is the axial maximum of amplitude furthest from the radiator, which occurs at

$$Z = (K^2 - \pi^2)/2\pi K = 1.435 \quad \text{for } K = 10.$$

This is also the point where the paths from the center and the edge of the piston differ by exactly $\lambda/2$, i.e., when the first Fresnel zone just fills the piston face. The graph shows that outside this boundary the wavefunction is farfieldlike, except that the amplitude minima are not zeros, thereby supporting this definition of the boundary. In fact, there are many other ways of defining the near/far boundary,[22] all essentially *ad hoc*. The appropriateness of a particular definition depends on the context, e.g., a definition appropriate to short pulses is given by Robinson *et al.*[19]

Our plots of cw amplitude agree quite well with Stenzel's plot,[23] except that Stenzel shows no evidence of the incipient null. They also agree qualitatively with plots[8,9] for larger values of a/λ. To our knowledge, no one has previously displayed the equiphase lines or detailed plots of the actual wavefunctions. However, Truell *et al.*[10] have presented some theoretical results by plotting graphs of amplitude and phase as functions of R for a few fixed values of Z. Despite their choice of $K = 226$ (our $K = 10$) their Figs. 2–14 and 15 appear consistent with our Fig. 3(a), (b), (c).

Some experimental confirmation of the theory is provided by Dehn,[24] who *photographed* the near cw amplitude field of a circular piston radiator at $a/\lambda \simeq 28$ in a sequence of sections transverse to the axis. Chivers and Aindow[25] compare graphs of experimentally measured phase with those of Truell *et al.*, and find fairly good agreement if the comparison is based on an *effective* radius for their real radiator. They also observe that, contrary to the assumptions of many theoretical models, the nearfield of a piston radiator is planar only near 1.1 times the distance to the last axial amplitude maximum (giving $Z = 1.58$ in our case) and out to about half the (effective) piston radius. This observation is supported by our Fig. 3(c), except that the region of planarity appears to be centered at about $Z = 1.75$ rather than 1.58. Chivers and Aindow make the remark—very pertinent to our present study—that phase information in ultrasonic signals has traditionally been ignored, but is now becoming accessible.

III. THE GAUSSIAN ENVELOPE PULSE AND ITS DISLOCATIONS

For our main study we drive the piston with a pulse which is a small departure from a monochromatic signal, i.e., a quasimonochromatic pulse. A suitable model is a Gaussian envelope containing n cycles of the carrier within ± 1 standard deviation, where n is not too small. Hence we take

$$F(t) = \exp[(-t^2/2)(\omega/\pi n)^2]\exp(i\omega t).$$

Using the notation defined in the previous section, we compute

$$\begin{aligned}\Psi(R, Z, T) &= \Theta(1 - R)\exp\left(\frac{-(T - KZ)^2}{2(\pi n)^2}\right)\exp[i(T - KZ)] \\ &\quad + \frac{1}{\pi}\int_0^{\pi} d\varphi \left(\frac{R\cos\varphi - 1}{1 + R^2 - 2R\cos\varphi}\right) \\ &\quad \times \exp\left(\frac{-(T - KS)^2}{2(\pi n)^2}\right)\exp[i(T - KS)], \end{aligned} \tag{9}$$

where $S \equiv (Z^2 + 1 + R^2 - 2R\cos\varphi)^{1/2}$. On the axis this simplifies to

$$\begin{aligned}\Psi(0, Z, T) &= \exp\left(\frac{-(T - KZ)^2}{2(\pi n)^2}\right)\exp[i(T - KZ)] \\ &\quad - \exp\left(\frac{-(T - KZ')^2}{2(\pi n)^2}\right)\exp[i(T - KZ')], \end{aligned} \tag{10}$$

where $Z' \equiv (Z^2 + 1)^{1/2}$.

In the farfield

$$\begin{aligned}\Psi_F(\theta, \tau) &= \frac{2}{\pi K \sin\theta}\int_0^{\pi} d\varphi \cos\varphi \\ &\quad \times \exp\left(\frac{-(\tau + K\sin\theta\cos\varphi)^2}{2(\pi n)^2}\right) \\ &\quad \times \exp[i(\tau + K\sin\theta\cos\varphi)] \end{aligned} \tag{11}$$

for $\theta \neq 0$, and from (6)

$$\Psi_F(0, \tau) = \left(i - \frac{\tau}{(\pi n)^2}\right)\exp\left(\frac{-\tau^2}{2(\pi n)^2}\right)\exp(i\tau) \tag{12}$$

for $\theta = 0$, where $\tau \equiv \omega t - kr$ as in (8).

Computations were made with $K = 10.0$, as for the cw study in the previous section, and $n = 3$ (again to model the experimental work). We consider first the farfield limit (11) and (12), whose amplitude is shown in Fig. 4(a). At $\theta = 0$ it is virtually identical to the driving envelope

$$|F(t)| = \exp[-(\omega t)^2/2(\pi n)^2]$$

apart from a very slight broadening. From Eq. (12) we see that this is a consequence of the quasimonochromaticity of the pulse, which makes $\tau/(\pi n)^2$ much less than 1 for values of τ such that the Gaussian is significantly large.

The variation of $|\Psi_F|$ with $\tau \equiv (\omega t - kr)$ is due to the envelope; that with θ is due to the diffraction and is similar to that for cw as shown in Fig. 2(a). The main difference is that, as shown by Fig. 4(a) and (b), the dislocations occur only for $\tau \equiv (\omega t - kr) = 0$, instead of for all times as in the cw case, because τ does not factor out of the pulse wavefunction (11) and (12). However, Re $\Psi_F(\theta, \tau)$ is a continuous odd function

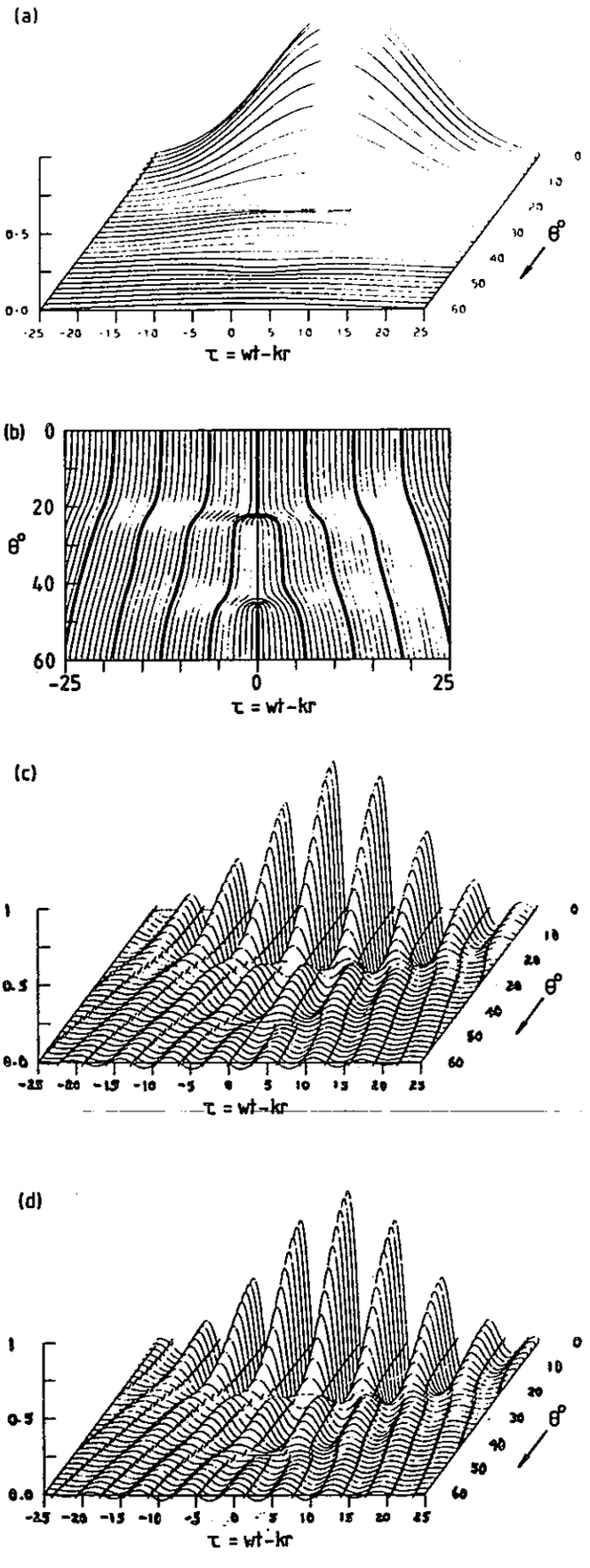

FIG. 4. Reduced farfield pulse wavefunction: (a) amplitude; (b) equiphase lines at 0 mod $\pi/4$—the heavy lines at $\pi/2$ mod 2π are for comparison with the cw case shown in Fig. 2(b); (c) real part; and (d) imaginary part.

of τ for all θ, which is why the dislocations occur *exactly* at $\tau = 0$ at angles such that Im $\Psi_F(\theta, 0) = 0$. Figure 4 shows that these angles are close to the cw null angles, as we expect from the continuity in n of (11) and (12) and the fact that a qm pulse (n large) is a small departure from its cw analog ($n \to \infty$). [This argument could be formalized by expanding the Gaussian in (11) producing effectively the perturbation theory.[7]] We found the precise angles of the farfield dislocation trajectories by computing Im $\Psi_F(\theta, 0)$ to a relative accuracy of 10^{-6} at a sequence of angles closely spaced around the cw null angles. From a graph, the values of θ giving zeros of Im $\Psi_F(\theta, 0)$ were found to be 22.67° and 44.88°. As a check, the method was also used to confirm the cw null angles to be 22.53° and 44.55°. The dislocations travel at angles shifted by very small but discernable amounts ($\simeq$0.7%) from the cw null angles; this shift would decrease if the pulse bandwidth were decreased.

The localization of the zeros has important consequences for the equiphase lines, changing the degenerate comb singularities of Fig. 2(b) into the two point singularities of Fig. 4(b), which have exactly the canonical pattern shown in Fig. 10 of Ref. 1. The effect of the phase singularities on the actual wavefunction is shown in Fig. 4(c) and (d). Consider the imaginary part of the complex wavefunction, as shown in Fig. 4(d), near $\theta = 60°$. Between $(\omega t - kr) = \pm 10$ we have three crests and two troughs. Near $\theta = 45°$ the central crest comes to an end and the troughs on either side coalesce into one central trough. Thus we have lost one crest and one trough in a symmetrical fashion, and the remaining crests and troughs have moved in to take up the vacated space. Near $\theta = 23°$ the process repeats itself with crests replaced by troughs; the central trough comes to an end and the two crests on either side coalesce into one central crest, so that we lose another crest and trough symmetrically.

The real part of the wavefunction, Fig. 4(c), shows exactly the same behavior, but here the crest and trough pairs disappear antisymmetrically. One can associate one wave front with one crest/trough pair (e.g., one could call the crests the wavefronts) and one sees that wave fronts come to an end near the phase singularities, as discussed in the Introduction. This occurs along circular loops about the axis such that there is one more wave front passing outside the loop than there is passing inside it.

We have seen that in the farfield the dislocations are static, which we define to mean stationary relative to the carrier wave, and occur exactly at the center of the pulse. Now we consider how they got there from the nearfield, where they were "born" and whether they are always static and at the center of the pulse. To this end we computed the nearfield wavefunction from (9) and (10) for times $T(\equiv\omega t)$ between 0 and 45. In Figs. 5–8 we display the amplitude, phase, real, and imaginary parts, respectively, of the complex wavefunction. The arrows indicate for reference where $Z = T/K$ (i.e., $z = \omega t/k$), which is where one would expect the geometrical pulse center to occur along the axis. Inside the near/far boundary (situated at $Z \simeq 1.4$) the diffraction is so complicated that it is impossible to say where the real pulse center is, but outside this boundary a meaningful pulse center becomes visible. It is useful to compare the pulsed

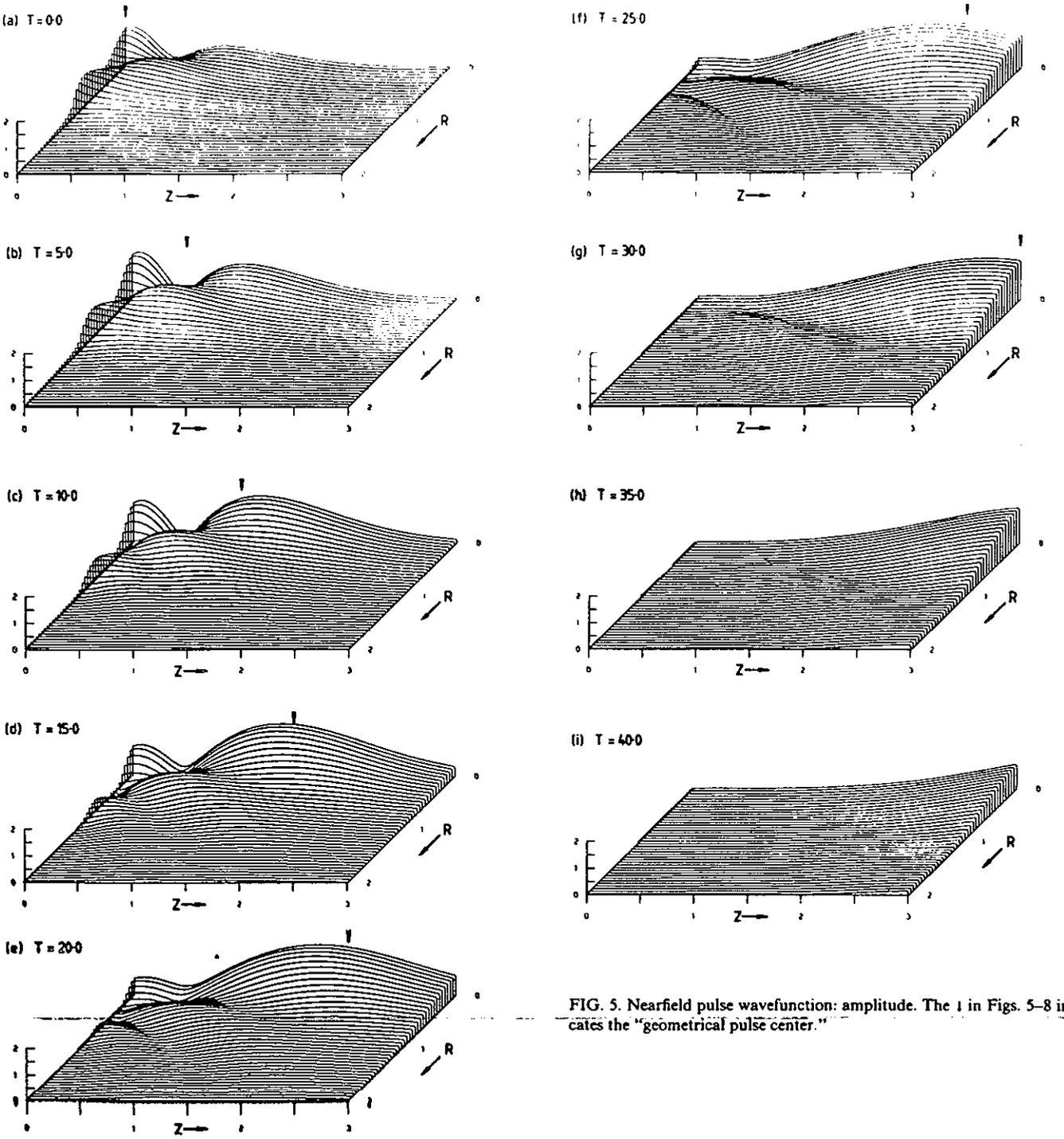

FIG. 5. Nearfield pulse wavefunction: amplitude. The ↓ in Figs. 5–8 indicates the "geometrical pulse center."

wavefield with the continuous wavefield as shown in Fig. 3.

At $T = 0$ [Figs. 5–8(a)] the wavefield is very similar to the cw field but with the features less pronounced, i.e., the valleys are only just visible and the axial null is replaced by a minimum at a height above zero, but in about the same place as the cw null. The equiphase lines are a smoothed-out version of the cw case without the singularity. At $T = 0$ the pulse is centered (geometrically) on the piston face and at any distance away from the piston the amplitude is only just beginning to grow. The smoothness of the wavefield suggests that the interesting diffraction phenomena in the cw field actually take time to build up. We shall see that as time progresses the wave fronts become twisted and tangled as the pulse propagates.

This can be understood by recalling, as first shown by Schoch,[26] that the field can be regarded as a plane-wave component if the field point is "over" the piston plus a field radiated by the rim—the two terms, respectively, in Eq. (2). The latter field is dominated by "replica pulses"[27]—see Appendix B. The two components arrive at different times. At early times when the radiated pulse is near the piston, the centers of the component pulses are well separated and they do not interfere much. As time progresses and the radiated pulse moves away from the piston the component pulses

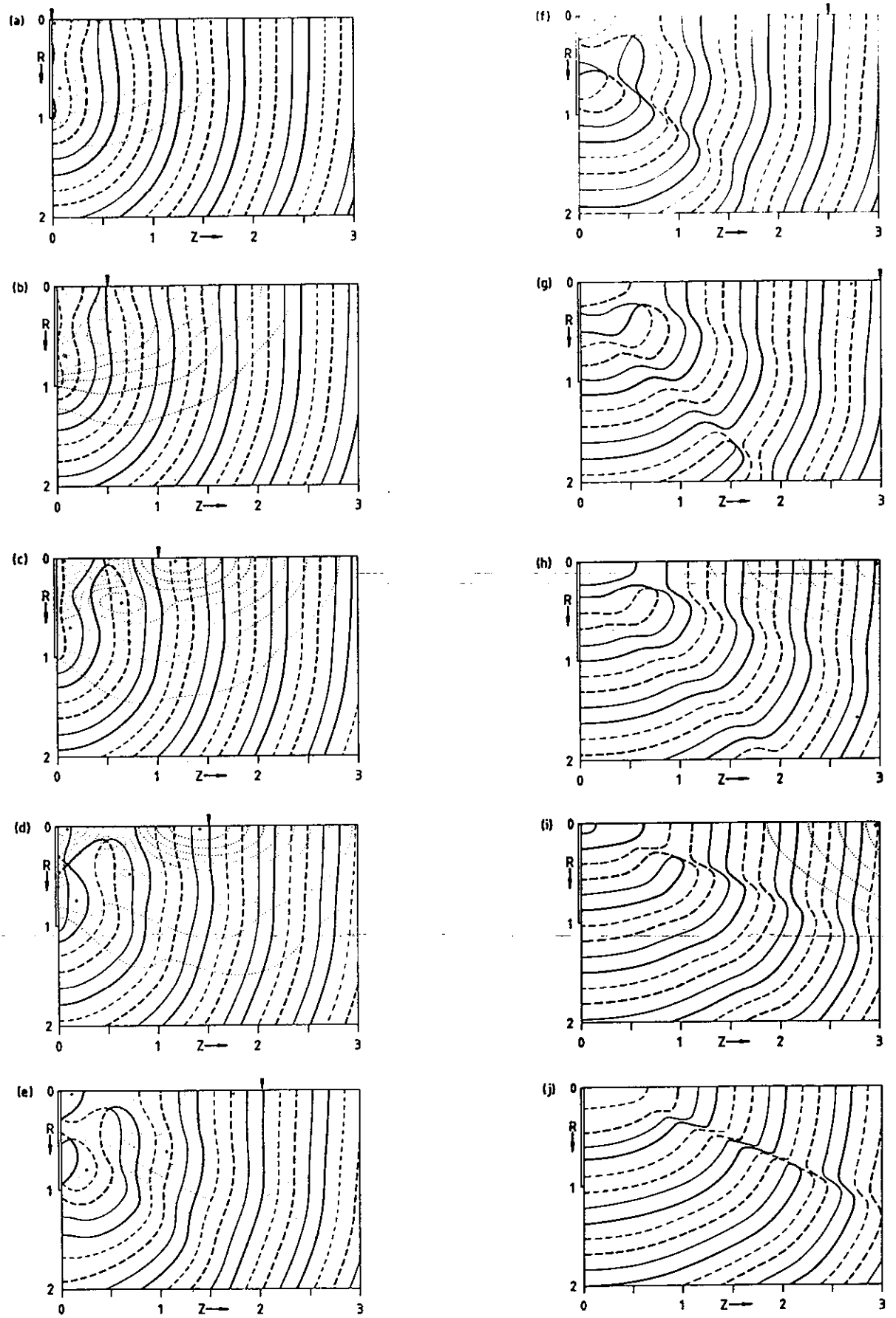

FIG. 6. Nearfield pulse wavefunction: equiphase lines (0:———; $\pi/2$: ——; π: — — —; $-\pi/2$: — — —) superimposed on the amplitude contours at 0 mod 0.2 (dotted), with local maxima marked by +.

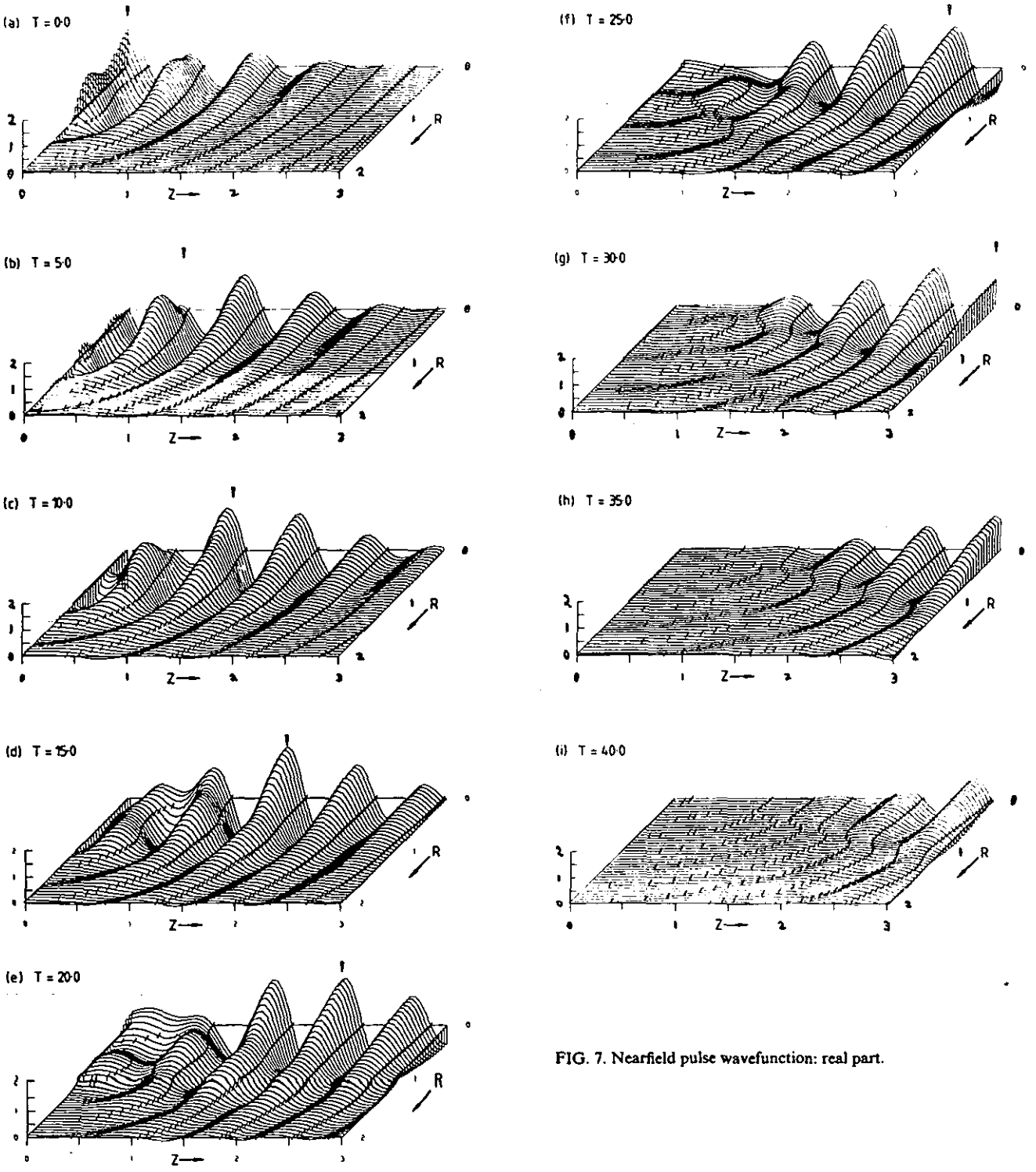

FIG. 7. Nearfield pulse wavefunction: real part.

overlap, and hence interfere, more strongly, leading to more prominent diffraction effects and hence more convoluted wave fronts. [Recall that the geometrical distance traveled by a pulse in Figs. 5–8 is equal to the distance of the arrow (↓) on the Z axis from the piston.] The transient buildup of the radiated field has been discussed in these terms before, mainly in the context of suddenly switching on a cw drive,[28,29] although not illustrated as we have done. Note, however, that our pulse envelope is smooth and infinitely extended, rather than having a sharp leading edge.

At $T = 5$ [Figs. 5–8(b)] the wavefield is developing more of the cw structure and the equiphase lines are moving in toward the axial cw null.

By $T = 10$ [Figs. 5–8(c)] the axial minimum has fallen to zero, and the equiphase lines coalesced, to produce a dislocation. At the end of this section we prove that the dislocation passes through the position of the axial cw null. We have not investigated this region in great detail, but we assume that a dislocation loop has been born by expanding from a point on the axis; the wave front has punctured and the

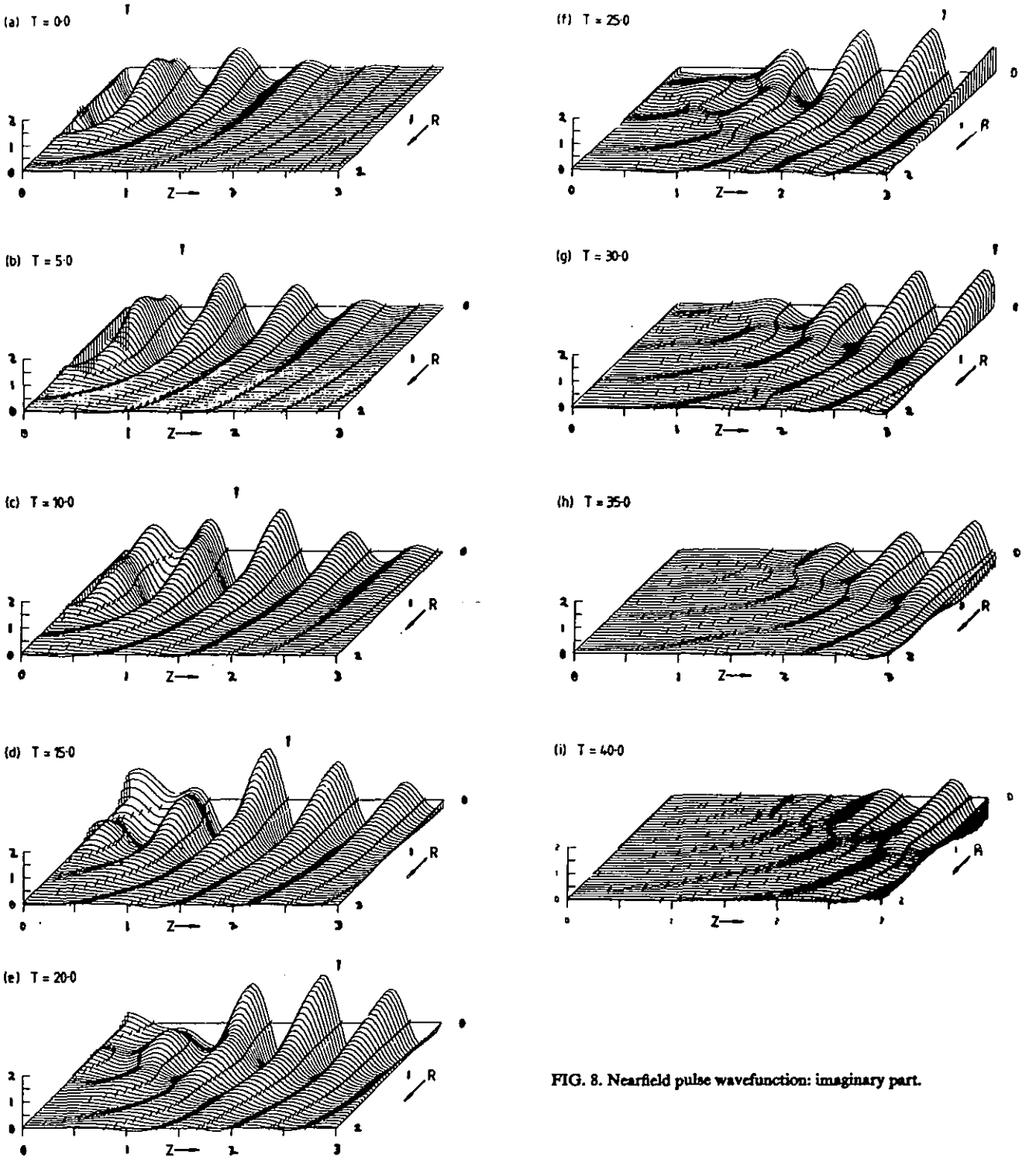

FIG. 8. Nearfield pulse wavefunction: imaginary part.

puncture opened into a circular hole. Figure 7(c) shows the first crest coming to an end near the axis [compare with Fig. 8(b), which is otherwise very similar].

At $T = 15$ [Figs. 5–8(d)] the zero of amplitude just off the axis is more clearly visible [in Fig. 5(d)], along with a new dip just in front of the piston. We see from the phase map, Fig. 6(d), that the dislocation near the axis has moved slightly further away from the axis (and the equiphase lines have rotated around it), and a new pair of dislocations, of strengths ± 1, have been born just in front of the piston face, almost exactly at a minimum of the cw amplitude. Figure 8(d) shows the crest just in front of the piston ending on one dislocation and then reappearing on the second. A pair of dislocation loops have been born which then climb apart, producing an annular tear in the wave front. Notice that the second birth occurs well into the tail of the pulse, and the first dislocation has dropped well back into the tail also. The center of the pulse is slightly behind its geometrical position, and seems to remain so until the farfield, where as we have seen it occurs at $\{\omega t - kr\} = 0$.

At $T = 20$ [Figs. 5–8(e)] we see a total of four dislocations, all dropping further into the tail of the pulse. Remember that in the farfield there are only two dislocations, which occur at the center of the pulse. The upper dislocation of the pair has moved back onto the piston face, where it will disappear (dislocations can only appear or disappear in pairs, or on a boundary, since their total strength is conserved[1]), and a new dislocation has appeared in the valley of the incipient cw farfield null discussed earlier. Notice how the equiphase lines are beginning to kink along the valleys of the cw amplitude.

By $T = 25$ [Figs. 5–8(f)] the two dislocations on the piston face have disappeared, but the remaining two have not moved very much. The center of the pulse is well beyond the near/far boundary, but the dislocations are still dropping back further into the tail. However, the equiphase lines are kinking very sharply along the second valley, which must portend something interesting. Figure 7(f) shows the two dislocations and the kinking of the wave fronts quite well.

At $T = 30$ [Figs. 5–8(g)] one immediately notices [see particularly Fig. 6(g)] that the second dislocation (at larger R) has jumped a long way, leaving the equiphase lines kinked the other way. The wave fronts have been torn and rejoined to the next one along; hence the name "glide" by analogy with the motion of dislocation lines in sheared crystals.[1] The equiphase lines around this dislocation now take on the canonical pattern as in the farfield, but the dislocation is still in the tail of the pulse.

At $T = 35$ [Figs. 5–8(h)] the second dislocation has moved with the pulse off the figure, but even by $T = 40$ [Figs. 5–8(i)] the first dislocation has not moved much. Figures 5(i) and 6(i) show just how far into the tail it has got. Finally, at $T = 45$ [Fig. 6(j) only], the first dislocation to be born finally begins to catch up with the pulse center, which it succeeds in doing only asymptotically. This dislocation drops so far into the tail of the Gaussian envelope pulse that numerical errors begin to affect the equiphase lines appreciably because of the very low amplitude.

We conclude this section by proving that an axial dislocation produced by any real positive definite pulse envelope can only occur at a cw null position. Inserting

$$F(t) = f(\omega t)e^{i\omega t}$$

into (3) gives, in the notation of Sec. II,

$$\Psi(0, Z, T) = f(T - KZ)e^{i(T - KZ)} - f(T - KZ_1)e^{i(T - KZ_1)},$$

where $Z_1 \equiv (Z^2 + 1)^{1/2}$. For Ψ to be zero the two terms being differenced must have the same amplitude and the same phase mod 2π. For real positive f the phase condition is identical to that for a cw null (in which case $f \equiv 1$); hence the proposition that the dislocation can only occur at a cw null position is proved.

The time of the dislocation at the null position $(0, Z)$ is given by

$$f(T - KZ) = f(T - KZ_1).$$

For *any* real $f > 0$ that is symmetric and monotonic decreasing away from the origin the unique solution at finite Z is

$$T = KZ' \equiv K(Z + Z_1)/2,$$

i.e., $t = [z + (z^2 + a^2)^{1/2}]/2c$

(where Z' was introduced in Sec. II). We see that the dislocation time is the mean travel time to the axial null from the center and edge of the piston. Within the class of pulses considered, the time (t) is quite independent of pulse shape or length, and also of the carrier frequency; it depends *only* on the piston radius. At the single axial null in our model the dislocation occurs at $T = 7.96$, which is consistent with the computed figures.

IV. BIRTH, DEATH, AND SKIP OF DISLOCATIONS

The study discussed in the previous section, of the near-field wavefunction over a fairly large region of space at widely spaced time intervals, has shown the general behavior of the dislocations. In this section we discuss some of the interesting events in more detail.

A. Birth of a pair of dislocation loops

This occurs near the piston face at $R \simeq 0.4$ between $T = 10$ and $T = 15$, as shown by Fig. 6(c) and (d): the mechanism is simply equiphase lines "pushing through" each other.

B. The incipient dislocation

At $T = 20$ there is a fourth dislocation close to the edge of the piston [i.e., at $R \simeq 1$, see Fig. 6(e)] whose existence is rather transient. Closer study reveals that it appears on the baffle plane just outside the piston, moves in an arc around the piston edge, and disappears on the piston face, as shown in Fig. 10. We conjecture that if K were increased so that there were three farfield nulls, then this dislocation would play a much more significant role and run off into the farfield.

C. The rapid dislocation glide by skip

Between $T = 25$ [Fig. 6(f)] and $T = 30$ [Fig. 6(g)] the dislocation at larger R jumps a long way, suggesting that some special mechanism, other than simple dislocation glide, might be involved. Figure 9 shows the process in greater detail; we have confined our attention to the equiphase lines of the wavefunction, because these convey the most information about the dislocations.

Before the jump [Fig. 9(a) and (b)] the structure becomes very complex. The equiphase lines kink more and more sharply so that they almost coalesce along a line, resulting in the birth of a new pair of dislocations of opposite signs ahead of the dislocation that is about to glide, at some time between $T = 25.5$ and 26.0. This pair then separates rapidly along the glide trajectory. Figure 9(a) shows the dislocation that is about to glide rapidly at the left, plus the newly born pair.

One of the pair of new dislocations approaches the original dislocation [Fig. 9(b)]. These two dislocations have equal and opposite strengths, and between $T = 26.2$ [Fig. 9(b)] and $T = 26.5$ [Fig. 9(c)] they meet and annihilate, leaving just the second member of the newly born pair as shown in Fig. 9(c). The original dislocation has "skipped" over the backward-moving member of the newly born pair and ended

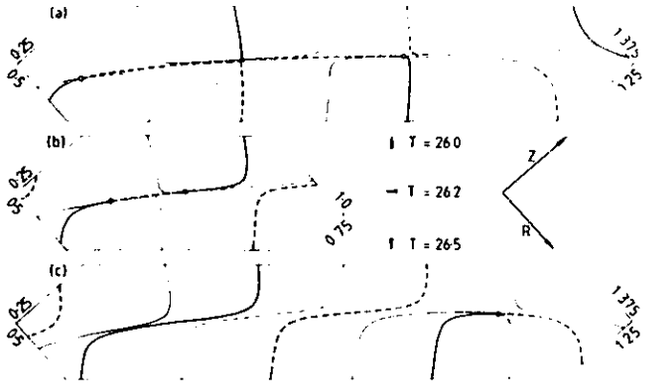

FIG. 9. The skip event. The figure shows equiphase lines (0: ———; $\pi/2$: ——; π: — — —; $-\pi/2$: — — —; $\pm\pi/4$, $\pm 3\pi/4$: · · · · ·) and the dislocations are marked by dots. The axes are rotated for compactness. Near the center of (a) a pair has been created; one of the pair approaches the original dislocation, which has opposite sign, (b) and annihilates it (c), leaving one dislocation, indistinguishable from the original, which appears to have "skipped over" a birth–death event and thereby glided very rapidly.

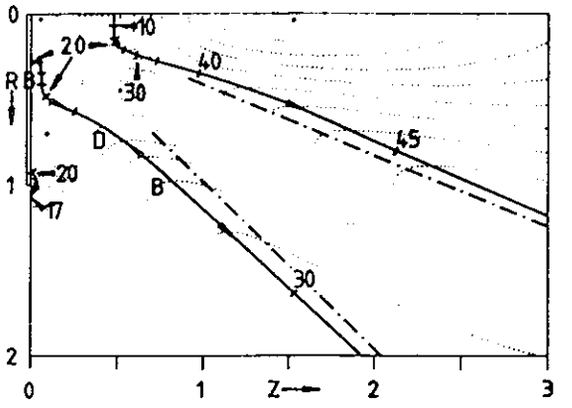

FIG. 10. The dislocation trajectories in the nearfield (solid), superimposed on the carrier amplitude contours at 0 mod 0.2 (dotted), with local maxima marked by +. The bars on the trajectories indicate the positions of the dislocations shown in Fig. 6, and the times at some points are explicitly shown. B and D indicate, respectively, births and deaths of dislocation pairs at interior points, and the arrows show the directions in which the trajectories are traversed.

up as what is really the other member of the pair. We have a continuous trajectory made up of (say) positive strength dislocations moving forward and negative strength dislocations moving backward.[1] The process is analogous to the interactions of elementary particles and their representation by Feynman diagrams.

After the jump the equiphase lines become progressively less sharply kinked and show the canonical structure.[1] We followed the dislocation as it slowly and smoothly caught up with the pulse center, and there is no evidence of any further jumps.

V. THE DISLOCATION TRAJECTORIES AND PERTURBATION THEORY

Figure 10 summarizes the information gathered so far by plotting the *trajectories* of the dislocations, i.e., the paths which they trace out as they move. The times at which they pass certain points are indicated, and the directions of motion are indicated by the arrows. The trajectories are superimposed on contours of the cw amplitude for the carrier of the pulse. This shows that, to a fair approximation, the dislocations are born near the two *minima* of the carrier amplitude and then travel away from them near to the bottoms of *valleys* [indicated by the curvature of the contour lines—see also Fig. 3(a)]. Two of the dislocations pass over the two saddle points and then run down the two valleys which lead into the farfield. Only these two "valley systems" are used—that joining the two amplitude minima is not.

That the dislocations in qm pulses should travel along lines close to which the amplitude of the carrier is, in some sense, minimal is not surprising. One may regard the effect of the modulation as pulling the already *low* cw amplitude down to *zero* pulse amplitude at some specific time. However, this is merely an *a posteriori* justification, not a theory of qm dislocations—one problem with trying to build a theory along these lines is the imprecision of the concept of valley (see also Ref. 7).

The method of study we have used is costly because of the computer time required to evaluate the pulse diffraction integral many times. We therefore evaluated the wavefunction only at rather widely spaced times and so incurred the risk of missing an interesting event that happened between two of these times. Our crude semi-empirical method, which consisted of computing the wavefunction at fixed times and then searching for dislocations by eye, could be refined by programming the computer to perform a multi-dimensional search for zeros. Apart from being algorithmically complex, such a search would only be reliable (or worthwhile) with a much smaller time interval than the five units we used here, so making it even more costly. With three nontrivial space dimensions it would probably be infeasible.

A better method of studying qm dislocations is provided by the perturbation theory developed by Wright and Nye.[7] This regards a quasimonochromatic pulse as a small perturbation of a continuous wave, and expands the wavefunction in a perturbation series in the pulse bandwidth. Truncating this series after the first order term and equating to zero gives nontrivial predictions for the behavior of the dislocations. Using the notation of Ref. 7 (except that their wavefunctions are the complex conjugate of ours) the results are most succinctly expressed in terms of the amplitude $M(\mathbf{r}, \omega)$ and phase $\varphi(\mathbf{r}, \omega)$ of the cw field, which may be represented as

$$M(\mathbf{r}, \omega)\exp\{i[\omega t - \varphi(\mathbf{r}, \omega)]\},$$

where $\mathbf{r}$ denotes spatial position, and we indicate all frequency dependences explicitly. We denote *derivatives with respect to frequency* ω by primes, and evaluate all functions at the carrier frequency ω_0. The surprising conclusion is that, to lowest order, the dislocation trajectories are contained in the set of points S satisfying

$$M'(\mathbf{r}, \omega_0) = 0, \quad M''(\mathbf{r}, \omega_0) > 0. \tag{13}$$

This result is *independent of the pulse shape*, although it is only valid in the qm limit (as the bandwidth tends to zero). It

states that *dislocation lines in qm pulses travel along the surfaces where the cw amplitude at the carrier frequency is minimal with respect to changes in frequency*. This prediction has been checked against a simple analytically soluble two beam model,[7] and against experiment,[13] and found to work very well.

Wright and Nye[7] show that the dislocations produced by a Gaussian envelope pulse will explore the *whole* of S, but that generally the extent of S traced out will depend on the shape of the pulse envelope. They also give formulae for the time at which a dislocation passes a given point on its trajectory, which again depends on the pulse shape, and it is here that the main subtlety of the perturbation theory appears. It is also worth remarking that it should be possible to apply the perturbation theory to features of qm pulses other than dislocations.

When the result (13) for the dislocation trajectories was applied to the present model, the results agreed within the plotting error with those shown in Fig. 10. This provides further confirmation of the perturbation theory, and also confirms that if we have missed any dislocation trajectories empirically then they are also missed by the perturbation theory—a coincidence which seems highly unlikely. A preliminary study of the times predicted by the perturbation theory suggests good agreement, but we shall not pursue this here. It is interesting to note that our Gaussian pulse envelope contained only three carrier cycles within ± 1 standard deviation of its center, which means that it is rather far from monochromatic; however, the perturbation theory still works well attesting to its robustness!

Two apparent coincidences emerge from the perturbation theory. The first is that the lines $M' = 0$ lie very close to the bottoms of valleys (when $M'' > 0$) and the tops of ridges (when $M'' < 0$) of the surface formed by the graph in r space of $M(\mathbf{r}, \omega_0)$ for some fixed $\omega = \omega_0$. This observation implies that the main effect of a small change in frequency is locally to shift M rigidly in space without any other significant change in the values of M. The second apparent coincidence is that $\varphi''(\mathbf{r}, \omega_0)$ is very small on S, and seems to be quite closely related to $M'(\mathbf{r}, \omega_0)$ over much, but not all, of the wavefield. In the two-beam model discussed in Ref. 7 all odd frequency derivatives of M and all even frequency derivatives of φ have exactly the same zeros. These relationships have very important (and useful) consequences for the perturbation theory, but their general status is still not clear.

VI. CONCLUSION

We have illustrated the theoretical discussions of wavefront dislocations[1,2,4,6,7] by displaying quasimonochromatic pulsed wavefields computed accurately from an exact integral representation of the wavefield of a model circular piston radiator. Our plots show the nature of the dislocations themselves, of their births and deaths, and of skip, which involves a total of three interacting dislocations. The dislocations are born near the minima, and travel along valleys, of the carrier amplitude; in fact, any kind of dip in the carrier amplitude graph seems to give rise to dislocations in a qm pulse. Our results are consistent with the perturbation theory,[7] which predicts that dislocations will travel close to the frequency minimum surfaces of the carrier amplitude.

This is by no means a complete study of the dislocation structure of this system. We have considered only a single carrier frequency and a single pulse shape and length. Our purpose was not to be exhaustive, but rather to examine *in detail* some typical realistic wave-front dislocations. The best approach to more general studies is probably to use the perturbation theory[7] as the basic tool, whereby *one computation* gives the approximate dislocation trajectories and times. Thus it would be feasible to investigate the effects of varying the carrier frequency and pulse shape. In a similar way it should be possible to study the behavior of, say, the local maxima of the pulse amplitude, which might be more immediately relevant to present remote sensing techniques.

ACKNOWLEDGMENTS

We thank Professor J. F. Nye and Dr. V. F. Humphrey for their interest and helpful discussions, Dr. G. Dangelmayr for pointing out the connection with nulls of antenna patterns and the referee for his constructive comments and for bringing some additional references to our attention. FJW thanks the SERC for financial support in Bristol, where most of the research was performed,[30] although the paper was prepared in London. This research was not supported by any military agency.

APPENDIX A: THE INTEGRAL REPRESENTATION FOR THE SOUNDFIELD

We sketch and discuss our derivation of Eq. (2) following Wright.[30] Certain aspects of this derivation have been presented before (e.g., Refs. 26 and 17), and Archer-Hall *et al.*[11] have recently derived a similar final result for the cw case. For the general context see the reviews by Harris[31] and Freedman.[32]

Using the coordinate system of Fig. 1, let ρ be a vector parallel to the baffle plane, ρ_0 a vector in the baffle plane, and let the displacement of the piston be decomposable as $G(\rho_0)F(t)$. Then if s is the distance from a source point at ρ_0 on the baffle plane to the field point at (ρ, z), the velocity potential wavefunction is given by

$$\psi(\rho, z, t) = \frac{1}{2\pi} \int\int_B d^2\rho_0 \frac{G(\rho_0)F'(t - s/c)}{s}, \qquad \text{(A1)}$$

where F' represents the derivative of the function F. This exact representation as a double integral over the baffle plane B is due to Rayleigh.[33] It is a Green's function solution of the inhomogeneous wave equation, with the integrand representing the "Huygens' wavelet" from each point of the radiator.

It is worth remarking that this problem is different in principle from that of diffraction of plane waves by a circular aperture, for which the wavefunction is not known *a priori* within the aperture. The two problems become equivalent only in the high-frequency limit when the Kirchoff approximation becomes valid—generally it is not only inaccurate[34] but not self-consistent.[35]

(A1) is conveniently rewritten as the convolution integral

$$\psi(\rho,z,t) = \int_{-\infty}^{\infty} ds'\, \hat{H}(\rho,z,s') F'(t - s'/c), \tag{A2}$$

where

$$\hat{H}(\rho,z,s') = \frac{1}{2\pi} \int\int_B d^2\rho_0 \frac{G(\rho_0)\delta(s' - s)}{s} \tag{A3}$$

is the impulse response,[31] which we evaluate analytically.

The circular symmetry of the system is introduced by setting $G(\rho_0) = G(\rho_0)$ with $\rho_0 = |\rho_0|$. Transforming to circular polar coordinates such that $\rho \cdot \rho_0 = \rho\rho_0 \cos\theta$ and noting that

$$\delta[s' - s(\theta)] = \sum_i [\delta(\theta - \theta_i)] \Big/ \left| \frac{\partial s}{\partial \theta} \right|,$$

where $\{\theta_i\}$ is all real solutions of $s' - s(\theta) = 0$, the angular integration may be performed and after a little trigonometry gives

$$\hat{H}(\rho,z,s') = H(\rho,s_0) u(s' - z),$$

where $s_0 = (s'^2 - z^2)^{1/2}$ is the distance between a source point and the projection of the field point onto the baffle plane, u is the unit step function, and

$$H(\rho,s_0) = \frac{2}{\pi} \int_{|\rho - s_0|}^{\rho + s_0} \frac{G(\rho_0)\rho_0 d\rho_0}{[(2\rho\rho_0)^2 - (\rho^2 + \rho_0^2 - s_0^2)^2]^{1/2}}. \tag{A4}$$

Using these formulae, (A2) may be re-expressed as

$$\psi(\rho,z,t) = -c \int_0^{\infty} ds_0 H(\rho,s_0) \frac{\partial F}{\partial s_0}[t - (s_0^2 + z^2)^{1/2}/c]. \tag{A5}$$

The integrand is clearly the contribution of a circular line source S of radius s_0 on the baffle plane, centered on the foot of the perpendicular from the field point.

For a rigid plane piston of radius a we have $G(\rho_0) = u(a - \rho_0)$ and (A4) may be evaluated analytically to give

$$H(\rho,s_0) = u(a - \rho - s_0) + u(s_0 - |\rho - a|) \times u[(\rho + a) - s_0] h(\rho,s_0), \tag{A6}$$

where

$$h(\rho,s_0) = \frac{1}{2} + \frac{1}{\pi} \arcsin \frac{a^2 - \rho^2 - s_0^2}{2\rho s_0}.$$

Explicitly, as s_0 varies the following three cases arise:

(i) if $\rho > a$ and $0 < s_0 < \rho - a$, or $s_0 > \rho + a$, then the source line S is outside the piston P and $H(\rho,s_0) = 0$;

(ii) if $|\rho - a| < s_0 < \rho + a$ then S is partly inside P and $H(\rho,s_0) = h(\rho,s_0)$;

(iii) if $\rho < a$ and $0 < s_0 < a - \rho$ then S is completely inside P and $H(\rho,s_0) = 1$ (as for an infinite plane radiator).

The form of the impulse response as a function of ρ is well illustrated in e.g., Refs. 9 and 19: it has different behavior as the projection of the field point lies inside ($\rho < a$), outside ($\rho > a$) or on the edge of ($\rho = a$) the piston.

Note that $h(\rho,\rho + a) = 0$; $h(a,0) = \frac{1}{2}$; and defining Θ to be the modified unit step function used in Eq. (2) gives $h(\rho,|\rho - a|) = \Theta(a - \rho)$ for all ρ. Then inserting (A6) into (A5) and integrating by parts gives

$$\psi(\rho,z,t) = \Theta(a - \rho) cF(t - z/c) + \frac{c}{\pi} \int_{|\rho - a|}^{\rho + a} \frac{ds_0}{s_0} \frac{\rho^2 - a^2 - s_0^2}{[(2\rho s_0)^2 - (a^2 - \rho^2 - s_0^2)^2]^{1/2}} \times F[t - (z^2 + s_0^2)^{1/2}/c].$$

To avoid the (integrable) singularity at both ends of the range, the integration variable is changed to φ defined by

$$s_0^2 = a^2 + \rho^2 - 2a\rho \cos\varphi$$

to give formula (2) of the text.

APPENDIX B: REPLICA PULSES

These were introduced by Freedman[27] as a means of *understanding* the structure of a radiated soundfield, and it is instructive to see how they emerge from our analysis for a general circularly symmetric piston radiator. Integrating (A5) by parts, assuming either $G(\infty) = 0$ for any real radiator, or $F(-\infty) = 0$ for any real pulse, gives

$$\psi(\rho,z,t) = cF(t - z/c)G(\rho) + c \int_0^{\infty} ds_0 \frac{\partial H}{\partial s_0}(\rho,s_0) F[t - (s_0^2 + z^2)^{1/2}/c]. \tag{B1}$$

Now if the whole baffle plane vibrates rigidly, so that $G(\rho_0) = 1$ for all ρ_0, then $H(\rho,s_0) = 1$ from (A4), and the second term in (B1) vanishes. Hence the first term in (B1) represents a plane-wave pulse emitted by the point on the baffle plane directly below the field point, and the second term represents the contribution from the rest of the radiator, a decomposition first effected by Schoch.[26]

The largest contributions from the integral in (B1) will come from discontinuities of H such as arise from the edges of the piston. Each discontinuity produces a "replica pulse," which is (generally) a distorted and delayed version of the primary pulse represented by the first term in (B1). Outside the piston ($\rho > a$) there is no primary pulse because $G(\rho) = 0$, so the dominant form of the soundfield consists purely of replica pulses.

The replica pulses appear particularly clearly on the axis of a circular piston, where $\rho = 0$. In the limit $\rho \to 0$, (A4) gives

$$H(0,s_0) = G(s_0) = u(a - s_0),$$

so that $$\frac{\partial H}{\partial s_0}(0,s_0) = -\delta(a - s_0)$$

and (B1) reduces to the simple axial form (3). In this high-symmetry position the two replica pulses merge into a single replica represented by the second term in (3). It is an undistorted copy of the primary pulse, but *inverted* and delayed: it corresponds to the "edge wave" from the rim of the piston. On moving into the farfield, the canceling effect of the replica differentiates the primary pulse (assuming F to be at least once differentiable) to give the farfield form

$$\psi(0,z,t) \sim (a^2/2z) F'(t - z/c) \quad \text{as } z \to \infty,$$

which is the axial form of (6).

The high-frequency limit of a cw field may be understood in terms of geometrical rays, some of which emanate

from the edge of the radiator. Dehn[24] has applied this idea to the cw field of the circular piston, and Kaspar'yants[28] to its transient switch-on. Edge rays underly Keller's powerful geometrical theory of diffraction,[36] which is much used in radio propagation problems. It is from the edge rays that the replica pulses contributing to a pulsed field arise. Stepanischen[18] has shown that the replica pulses produce interesting transient behavior at the cw nulls of a circular piston radiator, and Robinson *et al.*[19] have used empirically time-shifted replica pulses to find amplitude extrema. Beaver[12] displays computed wavefunctions showing the two replica pulses produced by the two opposite edges of a rigid circular radiator, and observes that

> "As the pulses move outward. . .the radiation zone on the piston becomes larger, and the discontinuity effects of the rims eventually overlap the main pulse, producing interference. The pulse amplitude is then more similar to the cw case. However, *distinct nulls cannot form because complete interference is not possible.*" (Our italics.)

While *fixed* nulls are certainly unlikely in any wavefield with nontrivial time variation, we have seen that *moving* nulls, which we call wave-front dislocations, certainly do occur in qm pulses. This should apply to Beaver's pulse types III and IV, although not his types I and II, to which his remarks were perhaps intended to be restricted.

[1]J. F. Nye and M. V. Berry, "Dislocations in wave trains," Proc. R. Soc. London Ser. A 336, 165–190 (1974).

[2]M. V. Berry, "Singularities in waves and rays," in *Les Houches Summer School 1980—Physics of Defects*, edited by R. Balian, M. Kléman, and J.-P. Poirier (North-Holland, Amsterdam, 1981), Vol. XXXV, pp. 453–543.

[3]M. E. R. Walford, "Glacier movement measured with a radio echo technique," Nature 239, 93–95 (1972). Note that the term "wave-front dislocation" was coined[1] later than this letter, which refers to "spatial fading pattern."

[4]J. F. Nye, "The motion and structure of dislocations in wavefronts," Proc. R. Soc. London Ser. A 378, 219–239 (1981).

[5]M. E. R. Walford, P. C. Holdorf, and R. G. Oakberg, "Phase sensitive radio-echo sounding at the Devon Island ice cap, Canada," J. Glaciol. 18, 217–229 (1977).

[6]F. J. Wright, "Wavefront dislocations and their analysis using catastrophe theory," in *Structural Stability in Physics*, edited by W. Güttinger and H. Eikemeier (Springer, Berlin, 1979), pp. 141–156.

[7]F. J. Wright and J. F. Nye, "Dislocations in diffraction patterns: continuous waves and pulses," Philos. Trans. R. Soc. London Ser. A 305, 339–382 (1982).

[8]J. Zemanek, "Beam behavior within the nearfield of a vibrating piston," J. Acoust. Soc. Am. 49, 181 (1971).

[9]J. C. Lockwood and J. G. Willette, "High-speed method for computing the exact solution for the pressure variations in the nearfield of a baffled piston," J. Acoust. Soc. Am. 53, 735–741 (1973).

[10]R. Truell, C. Elbaum, and B. B. Chick, *Ultrasonic Methods in Solid State Physics* (Academic, New York, 1969), p. 96.

[11]J. A. Archer-Hall, A. I. Bashter, and A. J. Hazelwood, "A means for computing the Kirchhoff surface integral for a disk radiator as a single integral with fixed limits," J. Acoust. Soc. Am. 65, 1568–1570 (1979).

[12]W. L. Beaver, "Sonic nearfields of a pulsed piston radiator," J. Acoust. Soc. Am. 56, 1043–1048 (1974).

[13]V. F. Humphrey, "Experimental Observations of Wavefront Dislocations in Pulsed Wavefields," Ph.D. thesis, Univeristy of Bristol, U.K. (1980); V. F. Humphrey and J. F. Nye, University of Bristol, U.K., in preparation.

[14]H. Steyskal, "Synthesis of antenna patterns with prescribed nulls," IEEE Trans. Antennas Propag. AP-30, 273–279 (1982).

[15]J. W. Strutt (Lord Rayleigh), *The Theory of Sound*, Vol. II (MacMillan, London, 1896), 2nd. ed. (reprinted by Dover, New York, 1945), Chap. XI; P. M. Morse, *Vibration and Sound* (McGraw-Hill, New York, 1948); S. N. Rschevkin, *Theory of Sound* (Pergamon, New York, 1963).

[16]NAG Mark 8 library routine D01AGF using adaptive Clenshaw–Curtis quadrature (Numerical Algorithms Group Central Office, Mayfield House, 256 Banbury Road, Oxford OX2 7DE, U.K.).

[17]O. G. Kozina and G. I. Makarov, "Transient processes in the acoustic fields of special piston membranes," Soviet Phys. Acoust. 8, 49–52 (1962).

[18]P. R. Stepanischen, "Transient radiation from pistons in an infinite planar baffle," J. Acoust. Soc. Am. 49, 1629–38 (1971).

[19]D. E. Robinson, S. Lees, and L. Bess, "Near field transient radiation patterns for circular pistons," IEEE Trans. Acoust. Speech Signal Proc. ASSP-22 395–403 (1974).

[20]*Handbook of Mathematical Functions*, edited by M. Abramowitz and I. A. Stegun (Dover, New York, 1964).

[21]Reference 15, Eq. 11–28.

[22]L. E. Kinsler and A. R. Frey, *Fundamentals of Acoustics* (Wiley, New York, 1962), 2nd ed., p. 176; R. J. Bobber, *Underwater Electroacoustic Measurements* (Naval Research Laboratory, Washington, DC, 1970), pp. 121–126.

[23]H. Stenzel, "Leitfaden zur Berechnung der Schallvorgänge," Berlin (1958); also displayed in Rschevkin (Ref. 15), p. 443.

[24]J. T. Dehn, "Interference patterns in the nearfield of a circular piston," J. Acoust. Soc. Am. 32, 1692–1696 (1960).

[25]R. C. Chivers and J. D. Aindow, "Preliminary measurements of ultrasonic phase distributions," Acoust. Lett. 4, 114–117 (1980).

[26]A. Schoch, "Reflections on the sound field of a piston membrane" (in German), Akust. Z. 6, 318–326 (1941).

[27]A. Freedman, "Sound field of plane or gently curved pulsed radiators," J. Acoust. Soc. Am. 48, 221–227 (1970).

[28]A. A. Kaspar'yants, "Nonstationary radiation of sound by a piston," Sov. Phys. Acoust. 6, 47–51 (1960).

[29]M. C. Junger and W. Thompson, Jr., "Fresnel-zone and plane-wave impedances on very large pistons," J. Acoust. Soc. Am. 38, 1059–1060 (1965); V. Mangulis, "The time dependent force on a sound radiator immediately following switch-on," Acustica 17, 223–227 (1966).

[30]F. J. Wright, "Wavefield singularities," Ph.D. thesis, University of Bristol, U.K. (1977).

[31]G. R. Harris, "Review of transient field theory for a baffled planar piston," J. Acoust. Soc. Am. 70, 10–20 (1981).

[32]A. Freedman, "Transient fields of acoustic radiators," J. Acoust. Soc. Am. 48, 135–138 (1970).

[33]Rayleigh (Ref. 15), Chap. XIV, Sec. 278, p. 107, Eq. (8), but note that he defines velocity potential with the opposite sign to us.

[34]R. D. Spence, "A note on the Kirchhoff approximation in diffraction theory," J. Acoust. Soc. Am. 21, 98–100 (1949); H. Levine and J. Schwinger, "On the radiation of sound from an unflanged circular pipe," Phys. Rev. 73, 383–406 (1948).

[35]H. Levine and J. Schwinger, "On the theory of diffraction by an aperture in an infinite plane screen I," Phys. Rev. 74, 958–974 (1948).

[36]For an introduction see the review by J. B. Keller, "Rays, waves and asymptotics," Bull. Am. Math. Soc. 84, 727–750 (1978).